CONF-820601--29

DE83 010781

PROBABILISTIC ASSESSMENT OF CRITICALLY FLAWED LMFBR PHTS PIPING ELBOWS

K. R. Balkey and I. T. Wallace

Westinghouse Electric Corporation
Advanced Reactors Division
Madison, Pa.

J. K. Vaurio

Fast Reactor Safety Technology
Management Center
Argonne National Laboratory
Argonne, Illinois

TITLE OF PAPER

ABSTRACT

One of the important functions of the Primary Heat Transport System (PHTS) of a large Liquid Metal Fast Breeder Reactor (LMFBR) plant is to contain the circulating radioactive sodium in components and piping routed through inerted areas within the containment building. A significant possible failure mode of this vital system is the development of cracks in the piping components. This paper presents results from the probabilistic assessment of postulated flaws in the most critical piping elbow of each piping leg. The criticality of calculated maximum sized flaws is assessed against an estimated material fracture toughness to determine safety factors and failure probability estimates using stress-strength interference theory. Subsequently, a different approach is also employed in which the randomness of the initial flaw size and loading are more-rigorously taken into account. This latter approach yields much smaller probability of failure values when compared to the stress-strength interference analysis results.

INTRODUCTION

Layout of the PHTS piping and components of a typical large LMFBR plant is shown in Figure 1. Loop arrangement is based on an "elevated loop" concept to provide protection against loss of coolant in the event of a sodium boundary failure in one of the loops. The PHTS performs the heat transport functions for all normal and certain abnormal modes of reactor operation.

The primary system hot leg piping from the reactor vessel outlet to the primary pump inlet in this study is nominally 36 in (91.4 cm) outside diameter by 0.5 in (1.27 cm) wall thickness. The remaining hot leg (crossover leg) piping from the pump discharge to the intermediate heat exchanger (IHX) inlet is 32 in (81.3 cm) outside diameter by 0.5 in (1.27 cm) wall thickness. The cold leg piping from the IHX to the reactor vessel inlet nozzle is also 32 in (81.3 cm) outside diameter by 0.5 in (1.27 cm) wall thickness. The hot and crossover leg piping is type 316 stainless steel (SS) and has a normal operating temperature of 950°F (510°C). The cold leg piping consists of type 304 SS and has a normal operating temperature of 670°F (354°C).

The piping is comprised of straight pipe runs and curved pipes and elbows, which are used for changes in direction of the piping system. The loops and bends in the horizontal piping runs provide the required flexibility to accommodate the thermal expansion of the system. Design, fabrication, and testing of the PHTS piping components, which comprise the sodium boundary, conform to Section III of the ASME Boiler and Pressure Vessel Code [1].

The most significant possible failure mode of the PHTS piping is the formation of significant cracks due to flaw propagation, resulting in large leakage or rupture of a piping leg. There are always some flaws which are significant and cannot be detected. A flaw with depth one-fourth the wall thickness, t, is initially chosen as a realistically conservative value since such a depth ratio finds consideration in Appendix G of Section III of the ASME Code, though it is not strictly applicable to this work. An initial flaw length of 3t is chosen to assure that the major effect of crack length is included, and surface defects are postulated since they are more severe than similar sized internal defects.

The fracture mechanics techniques used in this study and the analytical results are first summarized. Detailed structural reliability methods are then applied to illustrate an approach for the demonstration of inherent piping safety and reliability against the above postulated failure mode for a family of flaw sizes.

FATIGUE-CRACK GROWTH ANALYSIS METHODS AND RESULTS

This section presents a crack growth evaluation of piping legs of the typical PHTS. The objective of this analysis is to assess the potential growth of cracks, which are postulated to exist in the worst locations and orientations of the piping system under study, due to cyclic fatigue. The PHTS piping stress analysis results indicate that the elbow locations are the most highly stressed areas of the system. The thin wall of LMFBR PHTS piping results in elbow stress indices (multipliers) being on the order of 4 to 5 times greater than the respective values for light water reactor coolant loop piping. Therefore, the piping elbows become the critical locations in the primary system rather than the weld joints as reported for light water reactor piping crack growth studies [2].

The linear elastic fracture mechanics (LEFM) approach for calculating fatigue crack growth under cyclic loading is used [3]. The methodology employed in the evaluation is that detailed in Reference [4] and is briefly summarized below.

The approach used in this study is based on the well documented fact that the rate of cyclic crack growth (da/dN) is a function of the history of the effective stress intensity factor[1] at the crack tip. The crack growth rate relation considered to be applicable is [5]:

$$\frac{da}{dN} = C_o(K_{eff})^n \qquad (1)$$

where

$$K_{eff} = K_{max}(1-R)^m \qquad (2)$$

$R = K_{min}/K_{max}$, K_{max} and K_{min} are the maximum and minimum magnitudes of the stress intensity factor during a load cycle, and "m" is an experimentally verified factor to account for stress ratio effects. The function $C_o \cdot (K_{eff})^n$ is experimentally determined in the laboratory using conventional precracked specimens of the material of interest to define the

[1] The term "stress intensity factor", as used in the context of LEFM, must be distinguished from the same term, used in design requirements of the ASME Boiler and Pressure Vessel Code. As used here, the stress intensity factor is a characterization of the theoretical stress singularity predicted to exist at the tip of a crack in a perfectly elastic body under load.

fatigue-crack propagation behavior. The materials of the piping system under study have been extensively investigated to characterize the effect of various reactor operating conditions upon the rate of fatigue-crack growth. The crack growth rate curve applicable for a temperature range of $601 \leq T \leq 1,000^{\circ}F$ ($317^{\circ} \leq T \leq 538^{\circ}C$) as given in Figure 3 of Reference [4] is chosen for the flaw propagation analysis.

The cracks considered are assumed to be two-dimensional semi-elliptical surface flaws as shown in Figure 2. Since the crack geometry can be fully described by two dimensions, only growth in the depth direction (a) and in the length direction (2c) needs to be considered presuming self-similar growth. Therefore, stress intensity factors at points A and C (Figure 2) are required. Both membrane tension and linear bending loads are considered in the region of the crack. The equations for the stress intensity factors at points A and C on the crack front are expressed in the form:

$$\left.\begin{aligned} K_{A_{max}} &= \sigma_{b_{max}} \sqrt{\pi a}\, f_A\,(a/c,\ a/t) + \sigma_{m_{max}} \sqrt{\pi a}\, g_A\,(a/c,\ a/t) \\ K_{C_{max}} &= \sigma_{b_{max}} \sqrt{\pi a}\, f_C\,(a/c,\ a/t) + \sigma_{m_{max}} \sqrt{\pi a}\, g_C\,(a/c,\ a/t) \\ K_{A_{min}} &= \sigma_{b_{min}} \sqrt{\pi a}\, f_A\,(a/c,\ a/t) + \sigma_{m_{min}} \sqrt{\pi a}\, g_A\,(a/c,\ a/t) \\ K_{C_{min}} &= \sigma_{b_{min}} \sqrt{\pi a}\, f_C\,(a/c,\ a/t) + \sigma_{m_{min}} \sqrt{\pi a}\, g_C\,(a/c,\ a/t) \end{aligned}\right\} \quad (3)$$

where $\sigma_{b_{max/min}}$ and $\sigma_{m_{max/min}}$ are the maximum/minimum linear bending and membrane tensile components of stress acting transverse to the plane of the crack. The plate thickness (or pipe wall) is expressed as t. The influence of crack shape (a/c) and relative crack depth (a/t) are expressed through the f(a/c,a/t) and g(a/c,a/t) functions for the bending and tensile load conditions respectively as related in Ref. [4].

The stress intensity factors defined in equations (3) along with the f(a/c, a/t) and g(a/c, a/t) functions are generated from solutions obtained for flat plates. Curvature correction factors to these solutions for cylindrical shells are available. However, these factors are insignificant at crack depths less than seventy per cent of the wall thickness for piping components with dimensions similar to the PHTS pipe dimensions under study [6]. The effect of curvature is therefore not considered in the calculations since extensive end-of-life flaws did not develop.

Appropriate stress values, which include the critical load combinations and stress histograms for key selected duty cycle events, are input to the above fracture relationships along with the postulated initial defect (1/4t deep, 3t in length) to determine the crack growth amounts in the most severely loaded elbows of each piping leg. (An example of a load event stress histogram is given in Table 1 of Reference [4]). The stresses are applied to axially oriented flaws on the inside and outside surfaces of each elbow. Referring to Figure 2, the tensile membrane and bending stresses are superimposed in the hoop direction and act transverse to the plane of the crack, which is normal to the pipe (plate) surface. The axial stresses, being much less than the corresponding hoop stress values, are ignored in the analysis. Inside and outside surface flaws are evaluated because of the different operating environments and the reversal in thermal transient stresses.

Applying the stress cycles in a conservative and representative manner, the crack propagation analyses yielded the following results:

- The defects do not grow extensively during the load history for any of the cases studied. $a_{final} = 1.13\ a_{initial}$ for the highest case.
- The smallest crack growth occurs in the piping leg without pressure loadings.
- The outside surface cracks propagate significantly further than the inside surface cracks for each of the three piping leg elbows studied. The assumption of an aggressive air environment rather than the actual relatively inert nitrogen atmosphere for the outside surface cracks is the main reason for this phenomenon.
- Most of the crack extension, although small, occurs during either low cycle/high stress seismic events or high cycle/low stress load cases for all six crack situations. Additionally, the maximum applied stress intensity values in each crack situation are related to seismic events. This domination by earthquake loadings becomes important in the reliability assessment portion of the study.

SAFETY AND RELIABILITY ASSESSMENT

The criticality of the above calculated maximum sized flaws are now assessed against estimated material fracture toughness values to determine the factors of safety and probabilities of failure for the PHTS piping legs. Although crack propagation itself does not constitute failure, it is considered so in this safety and reliability assessment in an indirect manner. Flaw growth proceeds to failure if either the critical stress intensity, the critical flaw size, or the critical number of life cycles associated with the flaw is reached. In the above crack propagation analyses the worst loading event is applied to the maximum crack size, which grows to this configuration from application of the other significant duty cycle events during plant life, to obtain the maximum stress intensity for each crack situation studied. These maximum stress intensity values rather than the critical flaw sizes or life cycle values are used in the safety and reliability calculation since the latter parameters cannot be readily determined. The maximum stress intensity values range from 23.8 ksi $\sqrt{in}$ for the most severly loaded cold leg elbow to 35.2 ksi $\sqrt{in}$ for the critical hot leg elbow.

Critical material toughness values are determined prior to comparing them against the maximum applied stress intensities. Stress-strength interference theory is initially applied to estimate the failure probabilities. Subsequently, a more elaborate procedure is employed which includes several random variables in the determination of failure probability values.

Critical Toughness Determination

Because of the high toughness to yield strength ratio for annealed types 304 and 316 SS, the critical value of toughness, K_{Ic}, cannot be determined from LEFM testing. The test specimen would have to be immense to meet the LEFM testing requirements. Therefore, K_{Ic} must be determined from J_{Ic}, the critical value of Rice's J-Integral [7], resulting from elastic plastic fracture mechanics testing [8].

The toughness data reported for the materials and operating temperatures of interest are sparse and most of them exhibit a significant degree of scatter. These characteristics are depicted by the toughness data for annealed type 304 SS base metal given in Figure 3 [9]. The scatter in the data are due to the fact that the results are generated for different product forms, specimen configurations, and testing and data reduction techniques. This scatter could be narrowed by deleting some of the data on the basis of a recommended procedure for "valid" J_{Ic} toughness testing. However, this would further reduce the small quantity of available data. While available J_{Ic} values for 304 SS are not entirely satisfactory, there seems to be no means of improving the data at this time.

Reference 9 reports that toughness data for the 316 SS are more sparse than the 304 SS data, are scattered, and do not even border on the temperature ranges of the hot and crossover leg piping. However, a comparison of the J_{Ic} values for types 304 and 316 material, as shown in Figure 3, shows

316 SS to have a toughness approximately the same or slightly higher than the 304 SS values at the same respective temperatures. Therefore, it is assumed that the safety factor and probability of failure calculations can be carried out using 304 SS toughness data for 316 material even at temperatures higher than 600°F (315°C). This should be conservative particularly if the lower bound 304 SS toughness values are used.

Regarding the temperatures of interest, all of the data shown in Figure 3 are below the 950°F (510°C) normal operating temperature of the hot and crossover legs. An appropriate extrapolation of the available J_{Ic} values is necessary, but the actual toughness trend is not obvious because of the scarcity and scatter of the data. Nevertheless, the available higher temperature J_{Ic} values are assumed to be applicable at the 950°F (510°C) temperature.

The five data points in Figure 3 at temperatures from 752°F to 830°F for the hot/crossover leg evaluation span a wide range of toughness values. The maximum value is nearly twice as large as any other value in the data set and lies well outside the range of the other four test results. Since this result appears to be an overly optimistic estimate of material toughness, it is eliminated from use in the calculation. Therefore, the mean values of toughness are estimated to be 1,928 in-lb/in^2 and 217.5 ksi $\sqrt{in}$ (241 MPa$\sqrt{m}$) for J_{Ic} and K_{Ic}, respectively. (Plane strain testing conditions have been assumed in the general relationship between J_{Ic} and K_{Ic}.)

As for the cold leg (670°F, 354°C), test data at temperatures from 600°F to 752°F in Figure 3 are employed in the calculation. The range in toughness values is judged to be reasonable. J_{Ic} = 1,830 in-lb/in^2 and K_{Ic} = 219 ksi$\sqrt{in}$ (243 MPa $\sqrt{m}$) are the estimated mean values of toughness.

Factor of Safety Calculation

The factor of safety is calculated using the following relationship:

$$\text{Factor of Safety} = \frac{K_{Ic}}{K_{MAX}}_{APPLIED} \qquad (4)$$

Inputting the maximum applied stress intensities from each crack analyzed and the above determined critical values of toughness into equation 4, the factors of safety are calculated to range from 6.2 to 9.2, which are very high values for the three piping leg elbows studied. However, these margins of safety against crack induced failure are probably optimistic considering the wide scatter in the material toughness data. The following probability of failure calculation takes this dispersion of data into account.

Probability of Failure Calculation Using Stress-Strength Interference Analysis

The maximum applied and critical stress intensities are now treated as random variables in the probability of failure calculation. In order to apply the stress-strength interference theory, the probability distribution functions of these random variables are required.

A statistical analysis of the data [10] yields the coefficient of variation of the fracture toughness for the hot/crossover and cold leg piping to be 0.32 and 0.25, respectively. The median values are 217.5 ksi $\sqrt{in}$ and 219 ksi $\sqrt{in}$, respectively. The fracture toughness values were then plotted on normal, log normal, and Weibull probability paper to determine if the data fit any of these common statistical distributions. The J_{Ic} and K_{Ic} values for either hot/crossover or cold leg materials do not fit well against any of the above distributions as shown in Figures 4 through 6. Since no apparent method exists for improving the toughness data, the normal distribution is assumed

for the interference analysis. Though neither toughness parameter fitted better than the other for any of the distributions, K_{Ic} values are used rather than J_{Ic} values for convenience.

The variability of the maximum applied stress intensity is a function of flaw size and plant loading (transients, earthquake accelerations, etc.) distributions. Since it is not possible to derive quantitatively the applied stress intensity distribution given the fact that the distributions of some of these input parameters are unavailable, a normal distribution is assumed. Reference 11 shows that the upper tail probabilities of several common statistical models (for example, log normal, Weibull, gamma, exponential) having the same mean, μ, and standard deviation, σ, are bounded from above by the upper tail probabilities of the normal distribution with the standard deviation doubled. Distributions are plotted in Reference 11 for coefficients of variation, $\frac{\sigma}{\mu}$, equal to 0.10 and 0.25 for the common statistical models studied. Since the coefficient of variation for the applied stress intensity is estimated to lie within the 0.10 to 0.25 range, a doubling of the coefficient of variation to 0.50 is judged to be an adequately conservative measure for calculating the probability of failure using stress-strength interference theory.

When the strength (K_{Ic}) and stress ($K_{MAX\ APPLIED}$) are normally distributed, the failure probability (Q) is given by [10],

$$Q = \bar{\Phi}(Z) \tag{5}$$

where $\bar{\Phi}(\cdot)$ is the standard Guassian cumulative function, and Z is the standardized normal variate.

$$Z = \frac{(\mu_{K_{Ic}} - \mu_{K_{MAX\ APPLIED}})}{\sqrt{\sigma_{K_{Ic}}^2 + \sigma_{K_{MAX\ APPLIED}}^2}} \tag{6}$$

where $\mu_{K_{Ic}}/\sigma_{K_{Ic}}$ and $\mu_{K_{MAX\ APPLIED}}/\sigma_{K_{MAX\ APPLIED}}$ are the mean/standard deviations of the critical and maximum applied stress intensities, respectively. The $\bar{\Phi}(\cdot)$ values for different Z values may be obtained from standard texts; for example, Table A-1 of Ref.[10].

Using the critical stress intensity data discussed earlier and the maximum applied stress intensities, coincident with a coefficient of variation equal to 0.50, the probabilities of failure per year for the PBTS piping are determined to range from 5.2×10^{-6} to 1.4×10^{-4}. These probabilities of crack induced failure for the three piping leg elbows studied are significant. However, the actual failure probabilities should be much less if the random variability of all the parameters involved are considered.

Since the maximum applied stress intensities resulting from seismic events dominate the risk, a more detailed procedure is now employed in the following section to consider the flaw sizes, stresses due to earthquakes, and critical stress intensity values as random variables. This latter approach yields much smaller probability of failure values when compared to the above stress-strength interference analysis results.

It should be mentioned that the unreliabilities are quite insensitive to the coefficient of variation for the maximum applied stress intensity because of the wide scatter in critical toughness values (see equation 6). This also proves to be true in the more detailed analysis.

Probability of Failure Determination Using an Alternate Approach

Earthquake loadings are determined to be the dominating events from the crack propagation analysis results. Therefore, the probabilistic part can be carried out as follows. Let P_{ij} be the probability that $a = a_i$ and $c = c_j$ $(i,j = 1, 2, \ldots)$ to generate a family of several representative flaws. Let Q_k be the probability of an earthquake that causes bending and membrane stresses $\sigma_b = \sigma_{bk}$ and $\sigma_m = \sigma_{mk}$ $(k = 1, 2 \ldots)$. Using the stress intensity relationships given in equations (3), it is possible to calculate values $K_{A_{max,\,i,j,k}}$ with a_i, c_j, σ_{bk}, σ_{mk} and similarly $K_{C_{max,\,i,j,k}}$, etc. Since it is essential to consider the critical stress intensity, K_{Ic}, as a random variable, let $r_\ell (\ell = 1,2, \ldots)$ be the probability that K_{Ic} is less than or equal to the largest value of $K_{A_{max,\,i,j,k}}$, $K_{C_{max,\,i,j,k}}$, etc.; for each flaw and earthquake intensity level studied. The final failure probability estimate in the critical elbow of each piping leg is:

$$P_F = \sum_i \sum_j \sum_k \sum_\ell P_{ij}\, Q_k\, r_\ell \qquad (7)$$

Distributions for the critical stress intensity values for the PHTS piping materials are given in the previous section. These normal distributions are used in the r_ℓ probability determination (determination of r_ℓ is discussed in detail in the numerical calculations). Initial flaw size and earthquake probability distributions are generated below. Following these determinations, the failure probability estimates are calculated for the most highly stressed elbow in each piping leg and results are presented and discussed.

Initial Maximum Flaw Size Probability Distribution. The initial flaw size density distribution in a piping component after inspection should be directly related to the maximum flaw size density prior to inspection and to the probability of non-detection for the various inspection techniques employed. The nature of the required data is the initial flaw distribution prior to inspection and the statistical reliability of the applied non-destructive examination (NDE) methods. Ideally, both distributions should be a function of bivariate crack size distribution. Since relevant applicable data essentially do not exist for this case, initial flaw size probabilities are developed based upon a univariate approach, the crack depth.

Even for the univariate case, a lack of data using actual surveys exists at this time on both flaw characterization in metals and the reliability of NDE methods for the materials of prime interest. Rummel, et. al., [12] and Lemon [13] have performed work in this area on aluminum aircraft structural components to enhance aerospace technology. The reliability of NDE techniques are quantified in [12] and statistical concepts are presented in [13] to predict the in-service flaw size density distribution after inspection. Some parts of these studies are useful for the definition of defects and are employed in this PHTS piping reliability assessment.

The work by Lemon [13] centers on the determination of the initial in-service flaw distribution as a function of the reliability of the inspection techniques and the flaw size distribution prior to inspection. Lemon's development utilizes order statistics (that is, all flaws in a part are ordered by size from the smallest to the largest) and the most useful result is the derivation of the relationship of the maximum flaw size distribution after inspection-with-part-rejection to the maximum flaw size distribution prior to inspection. Often it is the case that only the largest flaws are known after inspection.

The probabilistic method derived by Lemon [13] has been used to calculate the maximum flaw size cumulative distribution for 0.5 in (1.27 cm) thick piping. The following assumptions were made:

1. Flaws in a part occur independently of one another.
2. The flaw size is unrelated to the number of flaws in a part.
3. There are fewer flaws of larger sizes in a part and many flaws of smaller sizes.
4. The probability density function of the initial flaw depth distribution is exponential.
5. The probability of having a flaw of depth 0.1 mm or greater is 0.9.
6. The flaw size of 3 percent or less of pipe wall thickness has a probability of detection of 0.0.
7. The probability of detecting a flaw depth in excess of 17 percent of the pipe wall thickness is no better than 0.997.

Assumption 3 was based on results of Kravchenko and Tursunov [14]. The exponential distribution of flaw sizes was previously used in an analysis by Becher and Pedersen [15], where it was stated that a flaw of 0.1 mm depth would "most certainly exist". Therefore, the probability of exceeding this flaw depth was taken to be 0.9 as given in assumption 5. Assumption 7 was based on results of NDE compiled by Holt [16].

As described by Lemon [13], the initial in-service flaw density function can be determined if the initial flaw size (depth) distribution and the probability of detection for the various NDE techniques are known. The flaw size depth distribution f(χ) was derived using the above considerations in assumptions 1 through 5 and is given by:

$$f(\chi) = 27.02e^{-27.02\chi} \quad 0<\chi<\infty \tag{8}$$

where χ is the flaw depth. The reliability of the combined NDE techniques was derived from the conditions noted in assumptions 6 and 7. The resulting probability of detection, P_d, as a function of flaw depth χ, was determined using a linear relationship between the limiting flaw depths in assumptions 6 and 7.

Lemon's expression for the distribution of the maximum flaw depth after inspection with part rejection is:

$$F_M(\chi|I, \chi_R) = \int_0^{\chi} K M \prod_{i=1}^{M} A_i \cdot B_i \cdot C_i \quad \text{for } o < \chi < \chi_R \tag{9}$$

where:

χ	=	flaw depth
I	=	inspection procedure
χ_R	=	rejection threshold - predetermined value for which a part is rejected if a flaw is found during inspection of depth equal to or greater than this value
K	=	a normalization constant
M	=	initial number of flaws per part
$F_M(\chi\|I, \chi_R)$	=	maximum flaw depth cumulative distribution after inspection-with-part-rejection and rejection threshold χ_R
A_i	=	probability that the i-th deepest flaw has a depth χ
B_i	=	probability that the i-th deepest flaw escapes detection given that it has depth χ
C_i	=	probability that the depth-ordered flaws i + 1 to M are detected and that each has depth less than χ_R given the i-th depth-ordered flaw has depth χ

In the analysis, $\chi_R = \infty$ is assumed. That is, all detected flaws are removed, but no parts are rejected. The maximum flaw size cumulative distribution is calculated as a function of the number of flaws, M. Results are given in Figure 7 for M=1 to M=10 for 0.5 in (1.27 cm) thick piping.

As M increases in Figure 7, the range of the distribution improves; and for sufficiently large values of M, the graphical representations should

coincide. Therefore, the distribution for M = 10 is chosen for the present work.

Table 1 gives approximate values of the post-inspection probabilities of existence for ten chosen flaw depths for the reliability assessment. These values represent the flaw probability densities at discrete intervals in the domain of the cumulative probability distribution given in Figure 7. Since the fracture mechanics relationships for the stress intensity factor calculation uses a two-dimensional crack geometry, the flaw length must also be included to complete a representative family of flaws. For each flaw depth (a_i) given in Table 1, flaw lengths (c_j) equal to 10 x a_i, 5 x a_i, and 1 x a_i are considered assigning the same probability of existence to all three crack shapes (long semi-elliptical to semi-circular). A value equal to 1/3 of the respective flaw depth probability is arbitrarily assigned to each of these flaws. This representation yields a family of 30 flaws spanning a wide range of configurations for the probabilistic analysis of the critical piping elbow in each piping leg.

Earthquake Probability Distribution. A feasible spectrum of earthquake probabilities as a function of intensity and geographic location is determined in this section for use in the PHTS piping probability of failure calculation. Hsieh, et. al., [17] have presented the probability of various levels of earthquake-induced ground accelerations for the Eastern United States (Figure 8); these probabilities have been used in the Reactor Safety Study [18].

For the present study, the ground acceleration values directly associated with the membrane and bending stresses induced by the operating basis earthquake (OBE) and safe shutdown earthquake (SSE) events are 0.15g and 0.30g respectively. From Figure 8 the annual probabilities associated with these seismic events are 1.2×10^{-3} and 1.9×10^{-4}, respectively for an Eastern United States plant site location. To obtain conservative values for a Western United States site location, the Eastern U.S. probabilities are increased by a factor of 3 [17]. The resulting earthquake probabilities used in the present work become 3.6×10^{-3}/year for the OBE and 5.7×10^{-4}/year for the SSE.

Numerical Calculations and Discussion of Results. For the three PHTS piping elbows under study, calculations are carried out to estimate the probabilities of crack induced failure from the application of two different earthquake intensities to a representative family of initial flaw sizes. Only one analysis is required for the critical elbow in each piping leg since the seismic stresses and material toughness values are similar (in the analysis) for both the inside and outside piping elbow surfaces.

Using the above generated data, a family of wide ranging defect sizes (a_i, c_j where i = 1, ..., 10 and j = 1, ..., 3) with associated probabilities, P_{ij}, are incorporated into the numerical computation along with the maximum seismic membrane and bending stresses (σ_{mk}^{max}, σ_{bk}^{max} where k = 1, 2) with related probabilities, Q_k. This input yields 60 flaw/earthquake combinations to be evaluated for each elbow. Maximum stress intensity values at the points of maximum depth and length on the crack front are determined by inputting these 60 sets of values into equations (3). The largest value of K_A^{max} and K_C^{max} for each of the 60 cases is selected to be K_{ℓ}^{MAX} where $\ell = 1, 2, \ldots 60$. The probabilities associated with these values are defined as follows:

$$P_\ell = P_{ij} Q_k \quad \text{where i,j,k have 10, 3, and 2 values respectively and thus } \ell \text{ has 60.} \tag{10}$$

Probabilities r_ℓ associated with K_{ℓ}^{MAX} exceeding the normally distributed material toughness parameter K_{Ic} are determined using the standardized normal variate defined as:

$$z_\ell = \frac{\chi - \mu}{\sigma} \tag{11}$$

where:

$\chi = K_{\ell_{MAX}}$

μ = mean value of K_{Ic}

σ = standard deviation of K_{Ic}

r_ℓ is given by,

$$r_\ell = \Phi(z_\ell) \tag{12}$$

where $\Phi(\cdot)$ is the standard Gaussian cumulative function.

Finally, the failure probability estimate for the critical elbow in each piping leg is generated by:

$$P_F = \sum_\ell P_\ell r_\ell \tag{13}$$

which is equivalent to Equation (7).

Failure probability estimates are summarized in Table 2 for the most critical elbow in each PHTS piping leg for the largest flaw/earthquake combinations and the cumulation of the entire family of representative defects and earthquakes studied. Results from the stress-strength interference analysis are also repeated. The main points of discussion from the analytical results are:

- The annual failure probabilities in Table 2 for the largest flaw/earthquake combination using the alternate approach show an improvement of about 5 orders of magnitude over the respective values calculated using stress-strength interference theory. The $\frac{a}{t} = 0.3$, $\frac{c}{a} = 10.0$ flaw/SSE loading combination clearly envelopes any crack and loading conditions evaluated in the previous analyses. Thus, use of the more rigorous alternate approach does significantly improve those values obtained by the interference analysis method.

- Long semi-elliptical flaws show higher failure probability estimates than semi-circular flaws, verifying that long shallow surface defects are more severe than semi-circular flaws.

- The failure probabilities for the mid-range defects ($0.08 < \frac{a}{t} < 0.015$) in combination with the lower earthquake intensities are the major contributors to the cumulative failure estimate for each elbow. This result occurs because of the high flaw probability density generated for the mid-range cracks, the high probability of occurrence defined for the OBE, and the wide distribution in material toughness. Although the results from the alternate approach yield more accurate and reduced failure probabilities, the cumulative values for each elbow are still fairly high from a structural reliability viewpoint. Additional work should be carried out to improve the initial flaw characterization for the materials of interest, to improve the seismic spectrum representation and, most importantly, to investigate the use of a different failure criterion in an attempt to further reduce the values. The use of the material flow stress rule is a possibility for a failure criterion.

The flow stress criterion checks failure caused by the remaining uncracked pipe cross-section being unable to support the applied loads. That is, pipe severance is assumed to be a result of net section plastic instability, which occurs when the net section stress (which can be determined using finite element analysis methods) exceeds the average material flow stress. The flow stress is generally taken as halfway between the yield and ultimate strengths to estimate the effects of strain hardening in the very ductile, tough austenitic stainless steel piping materials of interest.

The flow stress is probably a more representative failure criterion than the material toughness parameter, J_{Ic} (K_{Ic}). Assuming failure as a result of exceeding J_{Ic} is probably overly conservative since the materials of interest do not fail in a brittle manner as represented by use of this parameter.

The numerical results of the current work should not be taken as final since they are provided mainly to illustrate the technique. Discretization of continuous variables introduces errors that have not been quantitatively estimated in this application. For example, the representation of the seismic event spectrum by only two ground acceleration values may not be satisfactory. However, a refined spectrum is not expected to change results by orders of magnitude.

CONCLUSIONS

Initial semi-elliptical surface flaws are postulated to exist on the inside and outside surfaces of the most highly stressed elbow in each PHTS piping leg of a typical large LMFBR plant. These defects do not grow extensively under application of stress histograms conservatively representing the load history for defined key umbrella plant duty cycle events. Although crack propagation itself does not constitute failure, the maximum applied stress intensities associated with each defect are the important factors in the safety and reliability assessment.

The maximum applied stress intensities from the flaw growth analyses are compared against estimated critical material toughness values. High factors of safety were directly calculated, but marginal failure probabilities were determined using stress-strength interference theory because of the wide scatter in the measured critical toughness values.

Since the maximum applied stress intensities are shown to result from seismic events, a more detailed procedure considering the flaw sizes, the stresses due to earthquake, and the critical stress intensity values as random variables was employed. The respective failure probabilities from the interference analysis were improved by about 5 orders of magnitude for each elbow studied. In this detailed probabilistic assessment a representative family of initial flaw sizes spanning minute semi-circular defects to long deep semi-elliptical cracks was studied in conjunction with two earthquake levels of intensity (OBE and SSE). The failure probabilities for the mid-range defects in combination with the lower earthquake intensity (OBE) were major contributors to the cumulative failure probabilities for each elbow, rather than the large defect/large earthquake combination. The more accurate cumulative results for each elbow from the alternate approach are still fairly significant mostly due to the wide distribution in material toughness. In order to further reduce the values, additional work is recommended for improving the initial flaw characterization and the seismic spectrum representation and for investigating the use of a different fracture criterion (e.g., material flow stress rule). No means of improving current fracture toughness data seem to exist for the materials and temperatures of interest.

ACKNOWLEDGMENTS

This paper is based on work performed under the U.S. Department of Energy Contract DE-AM02-76CH94000 with the Westinghouse Electric Corporation, Advanced Reactors Division. The authors would like to thank Messrs. F. A. Lijewski and John Graham for their help and encouragement. Mr. G. Vaghasia is credited with generating the initial flaw size cumulative probability distribution curves. The computer programming assitance of Ms. M. Smith, a Westinghouse summer student employee from the University of Pittsburgh, is also gratefully acknowledged. A special word of thanks is due to Mrs. C. A. Hamill and Mrs. S. L. Gallowich for their efforts in preparing the manuscript.

REFERENCES

1. ASME Boiler and Pressure Vessel Code, Section III, Division 1, "Nuclear Power Plant Components," American Society of Mechanical Engineers, New York, N.Y., 1980.

2. "Large LOCA - Earthquake Combination Probability Assessment - Load Combination Program Project 1 Summary Report," NUREG/CR-1889, January 1981.

3. Paris, P.C., "The Fracture Mechanics Approach to Fatigue," in Burke, J.J., et. al., eds., Fatigue - An Interdisciplinary Approach, Racquette Lake, NY, August 13-16, pp. 107-132, Syracuse University Press, Syracuse, NY, 1964.

4. Balkey, K.R., "Effect of Significant Design Factors on Flaw Growth in an LMFBR Lower Core Support Structure," in Failure Prevention and Reliability - 1981, pp. 13-22, American Society of Mechanical Engineers, New York, 1981.

5. Janes, L.A., "The Effect of Stress Ratio Upon the Elevated Temperature Fatigue Growth Behavior of Several Reactor Structural Materials," HEDL-TME 75-20, Feb. 1975.

6. Mallet, R.H. and Nair, B.R., "Clinch River Breeder Reactor Plant Integrity of Primary and Intermediate Heat Transport System Piping in Containment," CRBRP-ARD-0185, Oct. 1977.

7. Rice, J.R., "A Path Independent Integral and the Approximate Analysis of Strain Concentration by Notches and Cracks," Transactions of the ASME Journal of Applied Mechanics, Vol. 90, 1968, pp. 379-386.

8. Paris, P.C., "Fracture Mechanics in the Elastic-Plastic Regime," in Flaw Growth and Fracture, ASTM Special Technical Publication, No. 631, pp.3-27, American Society for Testing and Materials, Philadelphia, 1977.

9. Konish, H.J., "Flaw Tolerance Implications of ASME Code Case N-47 and the Engineering Critical Assessment Method," WARD-SD-94000-10, Feb. 1981.

10. Lipson, C. and Sheth, N.J., Statistical Design and Analysis of Engineering Experiments, McGraw-Hill, New York, 1973.

11. Witt, F.J., "Practical Applications of Probabilistic Structural Reliability Analysis to Primary Pressure Systems of Nuclear Power Plants," Fourth International Conference on Pressure Vessel Technology, London, May 19-23, 1980, Paper C16-80.

12. Rummel, W. D., Todd, P.H., Rathke, R.A., and Castner, W.L., "The Detection of Fatigue Cracks by Nondestructive Test Methods," Material Evaluation, Vol. 32, 1974, pp. 205-212.

13. Lemon, G.H., "A Problem in the Distribution of Maximum Flaw Length After Inspection," Technometrics, Vol 16, 1974, pp. 577-583.

14. Kravchenko, D.F. and Tursunov, D.A., "Distribution of Internal Defects in a Sheet of Low-Carbon Structural Steel", Soviet Journal of Nondestructive Testing, Vol. 9, 1974, pp. 377-378.

15. Becher, P.E. and Pedersen, A., "Application of Statistical Linear Elastic Fracture Mechanics to Pressure Vessel Reliability Analysis", Nuclear Engineering and Design, Vol. 27, 1974, pp. 413-425.

16. Holt, A.B., "The Probability of Catastrophic Failure of Reactor Primary System Components", Nuclear Engineering and Design, Vol. 28, 1974, pp. 239-251.

17. Hsieh, T., Okrent, D., and Apostolakis, G.E., "On the Average Probability Distribution of Peak Ground Acceleration in the U.S. Continent due to Strong Earthquakes," UCLA-ENG-7516, March 1975.

18. "Reactor Safety Study--An Assessment of Accident Risks in U.S. Commercial Nuclear Power Plants, Main Report," WASH-1400, October 1975.

TABLE 1

INITIAL MAXIMUM FLAW SIZE PROBABILITIES

Flaw Depth to Thickness Ratio, a_i/t	P_{ij}
0.02	0.000
0.04	0.035
0.06	0.105
0.08	0.225
0.10	0.235
0.12	0.200
0.15	0.170
0.20	0.025
0.25	0.004
0.30	0.001

Note: For each flaw depth (a_i), flaw lengths (c_j) equal to 10 x a_i, 5xa_i, and 1xa_i are considered assigning the same probability of existence, $P_{ij}/3$, to all three crack shapes.

TABLE 2

PHTS CRITICAL PIPING ELBOW

PROBABILITY OF FAILURE ESTIMATES

PHTS Piping Leg	Probability of Failure (per year)		
		Random Variable Approach	
	Stress-Strength Interference	Largest Flaw & Earthquake[(a)]	Sum of All Flaws & Earthquakes
Hot	1.4×10^{-4}	1.0×10^{-9}	1.0×10^{-5}
X-Over	1.1×10^{-4}	8.1×10^{-10}	9.1×10^{-6}
Cold	5.2×10^{-6}	3.4×10^{-11}	3.4×10^{-7}

Notes: (a) Largest flaw dimensions are: $\frac{a}{t} = 0.3$, $\frac{c}{a} = 10.0$ and the largest earthquake is the SSE.

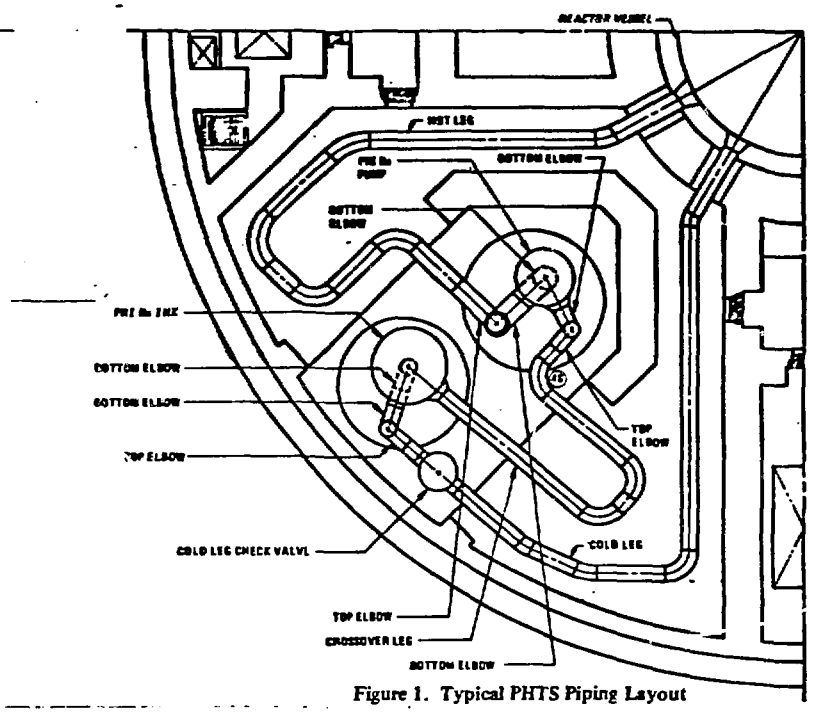

Figure 1. Typical PHTS Piping Layout

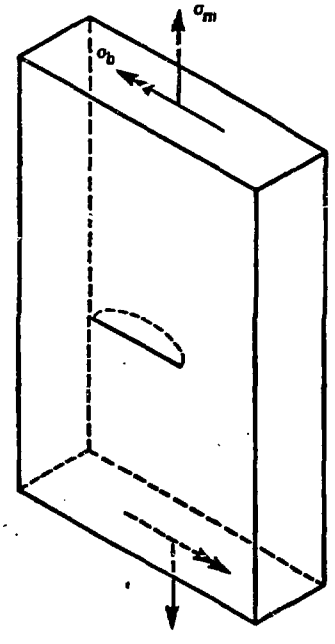

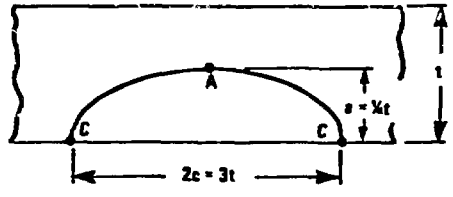

NOTE:

σ_m = MEMBRANE STRESS
σ_b = BENDING STRESS
a = CRACK DEPTH
2c = CRACK LENGTH
t = PLATE THICKNESS

Figure 2. Surface-Cracked Plate Subjected to Bending and Tension, with Detail of Crack Geometry

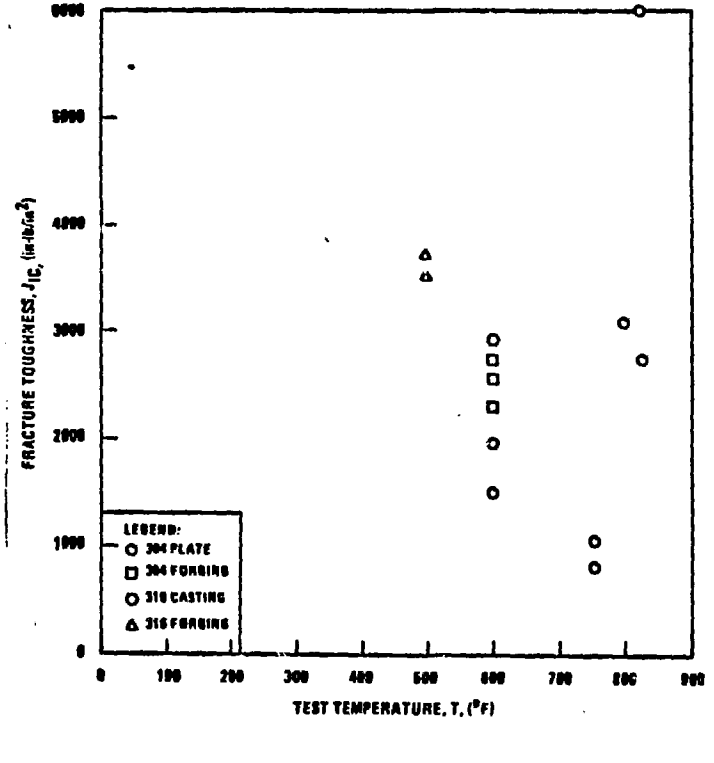

Figure 3. Fracture Toughness Vs. Test Temperature for Unirradiated Types 304 and 316 Stainless Steel Base Metal (1 In-Lb/In^2 = 0.175 KJ/m^2, $^0C = 5\ (^0F-32)/9$)

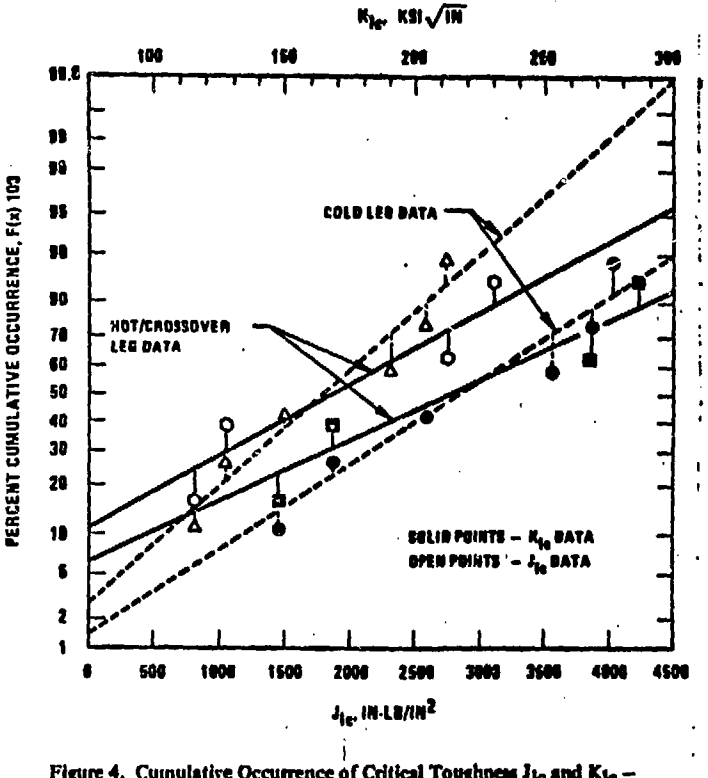

Figure 4. Cumulative Occurrence of Critical Toughness J_{Ic} and K_{Ic} – Normal Distribution (1 In-Lb/In^2 = 0.175 KJ/m^2, 1 Ksi$\sqrt{In}$ = 1.11 MPa$\sqrt{m}$)

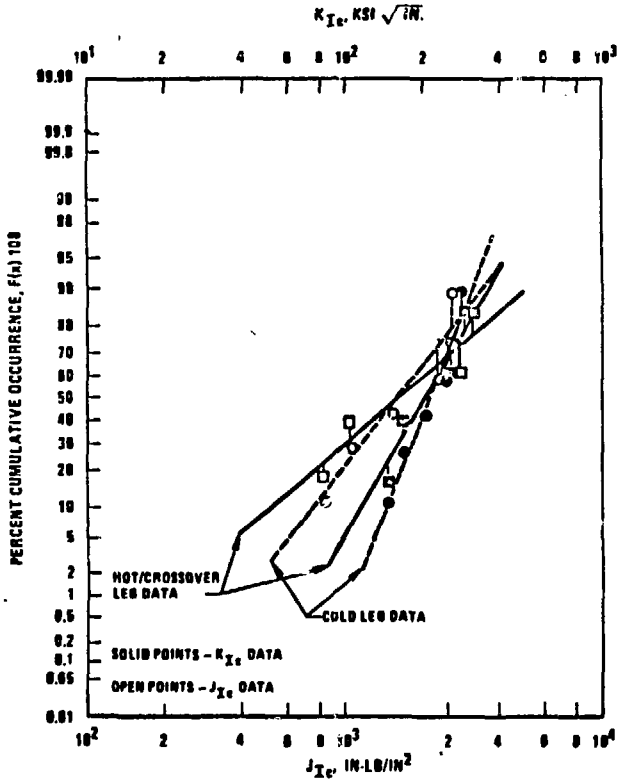

Figure 5. Cumulative Occurrence of Critical Toughness J_{Ic} and K_{Ic} – Log Normal Distribution (1 In-Lb/In^2 = 0.175 KJ/m^2, 1 Ksi$\sqrt{\text{In}}$ = 1.11 MPa$\sqrt{\text{m}}$)

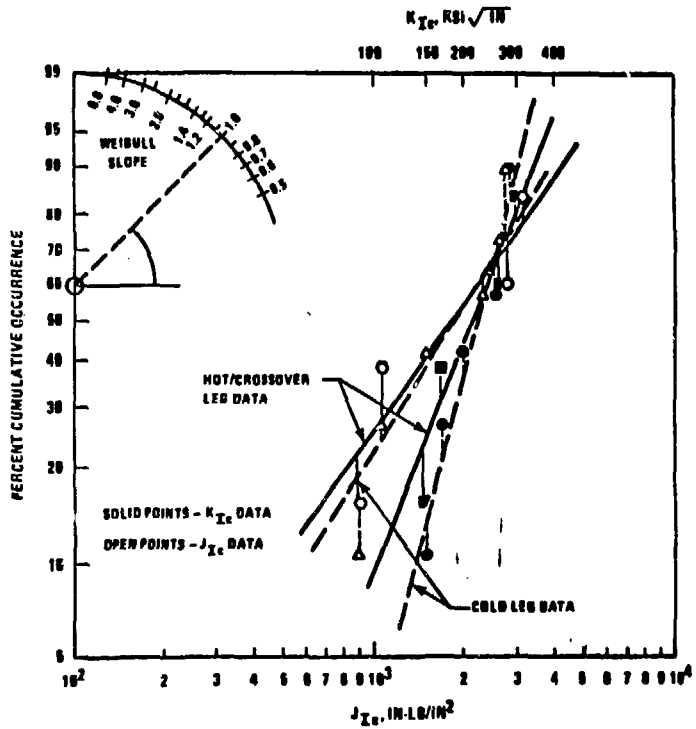

Figure 6. Cumulative Occurrence of Critical Toughness J_{Ic} and K_{Ic} – Weibull Distribution (1 In-Lb/In^2 = 0.175 KJ/m^2, 1 Ksi$\sqrt{\text{In}}$ = 1.11 MPa$\sqrt{\text{m}}$)

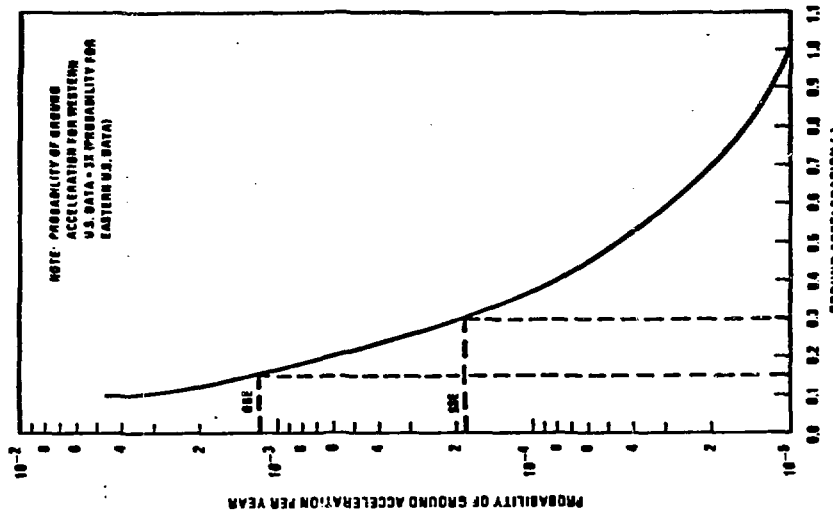

Figure 8. Eastern United States Ground Acceleration Probabilities

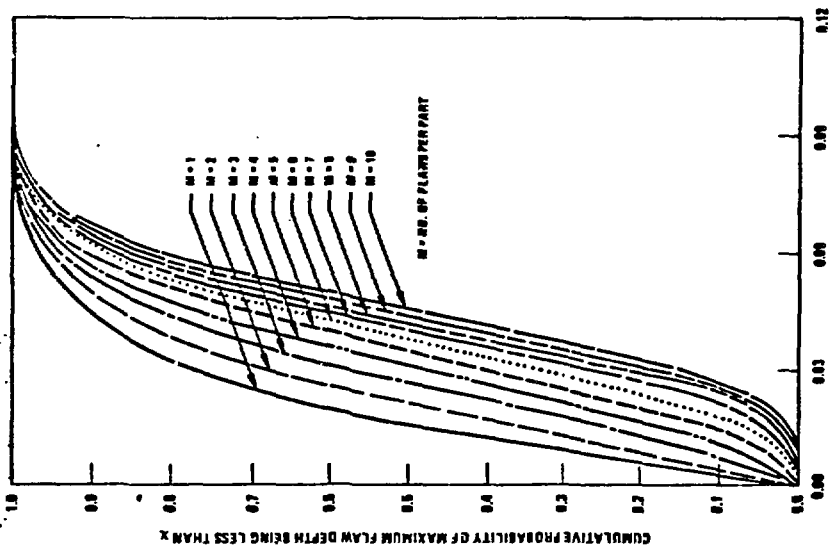

Figure 7. Cumulative Flaw Depth Distribution for 0.5 in. Thick Piping